THE ASTROPHYSICAL JOURNAL, 547:623–634, 2001 February 1

DEEP NEAR-INFRARED LUMINOSITY FUNCTION OF A CLUSTER OF GALAXIES AT $z = 0.3$[1]

S. ANDREON
Osservatorio Astronomico di Capodimonte, Via Moiariello 16, 80131 Napoli, Italy; andreon@na.astro.it
Received 1999 November 16; accepted 2000 September 27

ABSTRACT

The deep near-infrared luminosity function of AC 118, a cluster of galaxies at $z = 0.3$, is presented. AC 118 is a bimodal cluster, as evidenced both by our near-infrared images of lensed galaxies, by public X-ray *ROSAT* images, and by the spatial distribution of bright galaxies. Taking advantage of the extension and depth of our data, which sample an almost unexplored region in the depth versus observed area diagram, we derive the luminosity function (LF), down to the dwarf regime ($M^* + 5$), computed in several cluster portions. The overall LF, computed on a 2.66 Mpc^2 areas ($H_0 = 50$ km s^{-1} Mpc^{-1}), has an intermediate slope ($\alpha = -1.2$). However, the LF parameters depend on the surveyed cluster region: the central concentration has $2.6^{+5.1}_{-1.7}$ times more bright galaxies and $5.3^{+7.2}_{-2.3}$ times less dwarfs per typical galaxy than the outer region, which includes galaxies at an average projected distance of $\sim$580 kpc (errors are quoted at the 99.9% confidence level). The LF in the secondary AC 118 clump is intermediate between the central and outer one. In other words, the near-infrared AC 118 LF steepens going from high to low-density regions. At an average clustercentric distance of $\sim$580 kpc, the AC 118 LF is statistically indistinguishable from the LF of field galaxies at similar redshift, thus suggesting that the hostile cluster environment plays a minor role in shaping the LF at large clustercentric distances, while it strongly affects the LF at higher galaxy density.

Subject headings: galaxies: clusters: general — galaxies: evolution — galaxies: luminosity function, mass function — X-rays: galaxies

1. INTRODUCTION

The luminosity function (LF hereafter), i.e., the number density of galaxies having a given luminosity, is critical to many observational and theoretical problems (see e.g., Binggeli, Sandage, & Tammann 1988). For example, it is needed to interpret galaxy counts (e.g., Driver & Phillipps 1996), to compute the spatial covariance from the angular correlation function (e.g., Koo & Kron 1992), and to constrain the primordial power spectrum of density fluctuations (e.g., Ostriker 1993). From an observational point of view, the LF is the natural "weight" of several quantities since most statistical quantities are weighted on the relative number of objects in each luminosity bin. For example, the fraction of blue galaxies, which is the basic measure used for measuring the Butcher-Oemler effect (Butcher & Oemler 1978, 1984), is a (normalized) convolution, over the LF, of the color distribution at a given luminosity. Furthermore, owing to the role played by luminosity in the inclusion of the objects in the studied sample (faint objects are often excluded or underrepresented), the knowledge of the LF is fundamental to the calculation of the selection function and it is needed to derive the actual galaxy properties from the measured quantities. For instance, the large increase of the brightness of galaxies with z may be partially due to a z-dependent sampling of the LF (Simard et al. 1999).

Because of the central role played in many astrophysical problems, the optical LF of galaxies in clusters has been extensively studied (e.g., to cite just a few papers dealing with large numbers of clusters, Gaidos 1997; Valotto et al. 1997; Lumsden et al. 1997; Garilli, Maccagni, & Andreon 1999). However, not all wave bands carry the same information: optical filters are, with respect to near-infrared ones, more affected by short lived starburst events and thus better tracers of the metal production rate but worse tracers of the underlying stellar mass (Bruzual & Charlot 1993). It is therefore valuable to extend the LF measure to other bands. Near-infrared filters are useful in several aspects: with respect to optical filters they are less affected by internal and Galactic absorption, and their differential (type to type) K-corrections are quite small (up to $z \sim 1$) thus not altering the cluster content just because of an observational effect.

The present knowledge of the cluster near-infrared LF is quite fragmentary, and it is limited either to small areas at moderate depth (e.g., Barger et al. 1996; Trentham & Mobasher 1998; Aragon-Salamanca et al 1993) or to relatively large areas, but at bright luminosities (e.g., de Propris et al. 1999; Barger et al. 1998). This implies, for instance, that dwarfs galaxies are not sampled outside the cluster core. As a first step to overcome these drawbacks, we present in this paper the LF of a cluster of galaxies, AC 118, computed over one of the largest areas (in Mpc^2) and to a depth only rarely achieved for any cluster of galaxies.

AC 118, also known as Abell 2744 (Abell 1958; $z = 0.308$), is one of the most observed clusters at intermediate redshift. It was first studied by Couch & Newell (1984) on photographic plates, then low-dispersion spectroscopic data were acquired (Couch & Sharples 1987; Barger et al. 1996). For the very central region of the cluster ($r < \sim 9''$) *Hubble Space Telescope* images have been used for morphological studies (Couch et al. 1998; Barger et al. 1998) and mass determination through gravitational lensing experiments (Smail et al. 1997). Near-infrared (K'-band) photometry (Barger et al. 1996) of the very central region of this cluster at intermediate depth and with a coarse angular resolution (FHWM $\sim 1''.7$) is also available. Barger et al. (1996) present U and I photometry for the brightest K' sources. AC 118 shows an excess of blue galaxies (Couch &

[1] Based on observations collected at the European Southern Observatory, Chile, ESO N° 62.O-0369 and, in part, on observations with the NASA/ESA *Hubble Space Telescope*.

Newell 1984), commonly known as Butcher-Oemler effect (Butcher & Oemler 1978, 1984) and it is one of the clusters that triggered the discussion on whether the star formation rate increases or decreases during the galaxy infall in the cluster (Barger et al. 1996; Balogh et al. 1997, 1998).

The paper is organized as follows: in the next section, the data and the data reduction are presented. In § 3 the AC 118 LF is derived in a few cluster regions. The discussion and a summary are presented in § 4.

In this paper we assume $H_0 = 50$ km s^{-1} Mpc^{-1} and $q_0 = 0.5$. If $\Omega_\Lambda = 0.7$, $\Omega_M = 0.3$, AC 118 galaxies would be ~ 0.3 brighter. The main result of this paper, a clustercentric dependence of the LF, is independent on the cosmological parameters because all compared galaxies are at the same distance from us.

2. DATA AND DATA REDUCTION

2.1. *AC 118 Observations*

AC 118 observations were carried out at the 3.5 m New Technology Telescope (NTT) with SOFI (Moorwood, Cuby, & Lidman, 1998) on 1998 October 11, in the frame of an observational program aimed at deriving the fundamental plane at $z \sim 0.3$. SOFI is equipped with a 1024 × 1024 pixel Rockwell "Hawaii" array. In its large field mode the pixel size is 0.″292 and the field of view 5′ × 5′. The field was observed in the near-infrared K_s passband ($\lambda_c = 2.2\mu$; $\Delta\lambda \sim 0.3\mu$) during a photometric night with good seeing (FWHM < 0.″8). The total useful exposure time is 15,900 s, resulting from the co-addition of many short jittered exposures. Jittering was controlled by the automatic jitter template (described in the SOFI User Manual), which produces a set of dithered frames. Offsets were randomly generated within a box of 40″ × 40″ centered on the cluster center (α: 00 14 19; δ: −30 23 18, J2000). The effective exposure time of each individual AC 118 frame was 1 minute in K_s, resulting from the average of six exposures of 10 s each. Photometric calibration has been obtained by observing a few standard stars, interspersed with AC 118 observations, taken from the list of infrared NICMOS standard stars now published in Persson et al. (1998). The effective exposure time for standard stars was 100 s, given by exposures taken at five different array locations, each one being the average of 10 integrations 2 s long. Figure 1 shows the final K_s image of AC 118.

2.1.1. *Reset, Gain, and Illumination Corrections*

All images have been flat-fielded by flaton-flatoff. All pixels whose gain differs from the average by more than 30% have been flagged and not used in the image combining.

Hawaii chips have a special feature: after reset, the zero-level is not constant over the field and its amplitude depends on the total charge collected in the previous exposure. The variation of the zero-level is due to the fact that rows have not the same reset voltage after reset because resetting an Hawaii chip is a power demanding operation (MacKay et al. 1998). This pattern is additive and equal for all pixels in the same row since they are reset in parallel. This pattern is unimportant for science images, whose background is anyway spatially not uniform and variable in time. However, this spatial pattern and its time variation are important in the determination of the gain correction (i.e., of the flaton-flatoff). Figure 2 shows two typical zero-level patterns, and also their difference. This difference is ∼150 ADU with variations of ∼50 ADU from one row to another, which induces, if not accounted for, a photometric zero-point variation on the field at a few percent level. The zero-level has been measured using appropriate images (*special* flaton-flatoff frames), as suggested by C. Lidman (1998, private communication, now fully described in the SOFI manual). In the determination of the zero-level it is assumed that during the observations the lamp is stable; this assumption has been verified a posteriori, by comparing of a few series of such measurements.

In accurately reduced images the flux of a standard star should not depend on its location. In order to test the accuracy of the flat-fielding, a standard star has been observed 16 times, displacing the telescope pointing between each exposure by ∼80″, in such a way that the standard star appears on a grid 4 × 4, and its flux at the different positions on the chip has been measured. Two more stars were in the field of view and were also used for this test. Figure 3 shows the deviation from an ideal response (i.e., 1 everywhere), after gain correction and before any other correction. The measured flux is well within 1% from 1 in most of the sampled locations. The rms deviation is 0.7%, which, if not corrected for, would induce a 0.007 mag error. Part of the observed scatter is due to photometric errors on individual magnitude measurements, accounting for 0.005 mag. In just one location the measured flux differs by 2.4%. However, this outlier value could be partly due to a transient slightly hot/cold pixel unrecognized as such and uncorrected for. We recall that transient hot/cold pixels are recognized and corrected in the next phase, which combines images taken at different pointings.

Since the rms deviation from the mean is ∼0.7%, our images do not require a supplementary illumination correction, which is instead often considered in the reduction of near-infrared images. As a comparison, the rms deviation from the mean of the NICMOS 1 and 2 on *Hubble Space Telescope* is ∼2% (Colina, Holfeltz, & Richie 1998) and no illumination correction is included in the NICMOS pipeline reduction, to our best knowledge.

2.1.2. *Background Removal*

For the background subtraction a user-friendly software tool, Eclipse (Devillard 1997), has been used.

In the near-infrared, observers are faced with changes of the intensity, spectrum, and spatial shape of the sky. Nodding the telescope modulates the astronomical objects intensity (on a give pixel) more quickly than the background variation.

From a technical point of view, a high-pass filter will remove the slower changing background and will leave untouched the higher frequency astronomical signal. To make this operation effective, Eclipse scales time-adjacent images to the mean (or median) of the image that must be background-subtracted. In doing this operation, Eclipse assumes that the variation of the background is multiplicative and coherent over the whole field during the considered short time interval. Then, images are low-pass filtered in the time-line direction, using a filter 11 exposures large centered on the image whose background is to be subtracted, allowing a rejection of the faintest and of the three brightest pixels in order to take into account the existence of celestial objects, cosmic rays and intermitting hot/cold pixels. With this choice of the Eclipse settings, more bright pixels than faint ones are clipped during the sky determination. This is

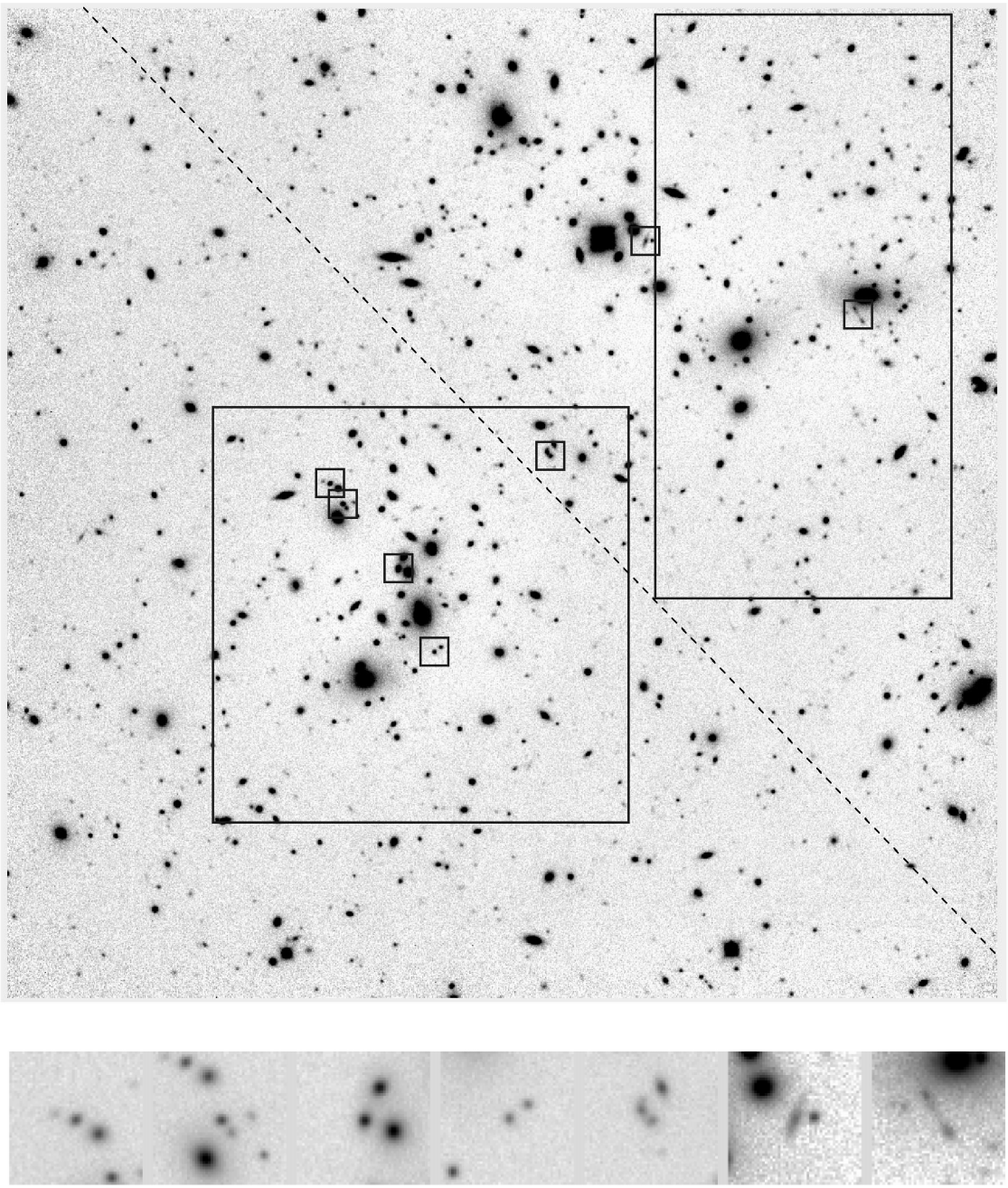

FIG. 1.—K_s-band image of AC 118. The field of view is $\sim 5' \times 5'$. North is up and east is to the left. The large boxes delimit the main and northwest regions (*large square and rectangle, respectively*). The "outer region" (see text) is the area below the slanted line and outside the large square. Small boxes mark the objects blended in Barger et al. (1996) image (*the six small boxes at east*) or gravitational lenses (*the two small boxes at west*). All them are magnified in the lower panel. The field of view of each zoom is 15″ on side.

the natural choice when, as in our case, sky pixels contaminated by sources have an asymmetric intensity distribution, i.e., when the number of sources with positive counts exceeds the number cold pixels. While pixel masking would be preferable, it is not available within the Eclipse software.

This operation gives the background, which is subtracted to the original flat-fielded image. We want to stress that no multiplicative scaling is applied to the image to be background-subtracted. We verified, by means of Midas pipelines developed by the author for the analysis of near-infrared images of the Coma cluster (Andreon et al. 2000), that Eclipse correctly performs this complex task.

2.1.3. *Photometric Calibration*

The air mass coefficient is computed by means of the science frames, due to the fact that AC 118 has been observed at several hour angles. We determine the air mass coefficient from the measure, on 190 out of 265 frames, of the apparent flux of a small galaxy (a possible early-type galaxy of AC 118) in an uncrowded region. The upper panel of Figure 4 shows the air mass dependence of the instrumental magnitude of the considered galaxy. The adopted value for the atmospheric absorption, 0.08 mag air mass^{-1}, is compatible with that derived from the observations of the (admittedly few, 5) photometric standard stars observed

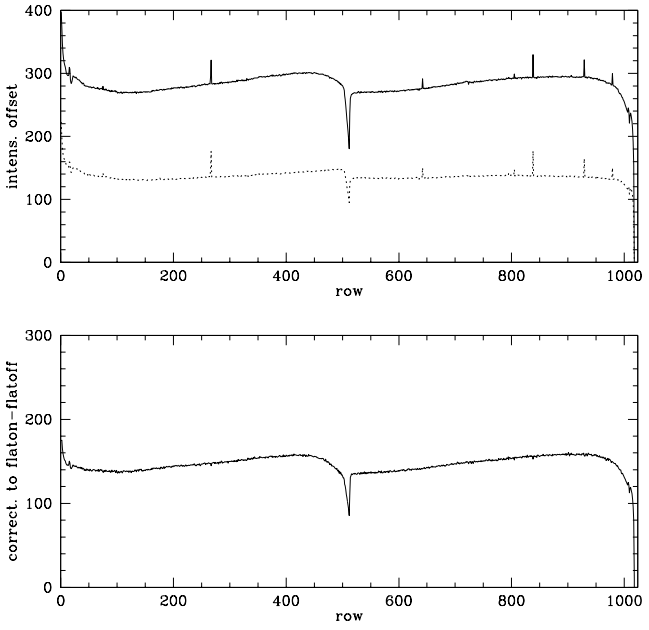

FIG. 2.—*Upper panel:* Zero-level of flaton (*solid line*) and flatoff (*dotted line*). Spikes are due to bad pixels and do not reflect real variations of the zero-level. *Lower panel:* Difference of the two zero-levels.

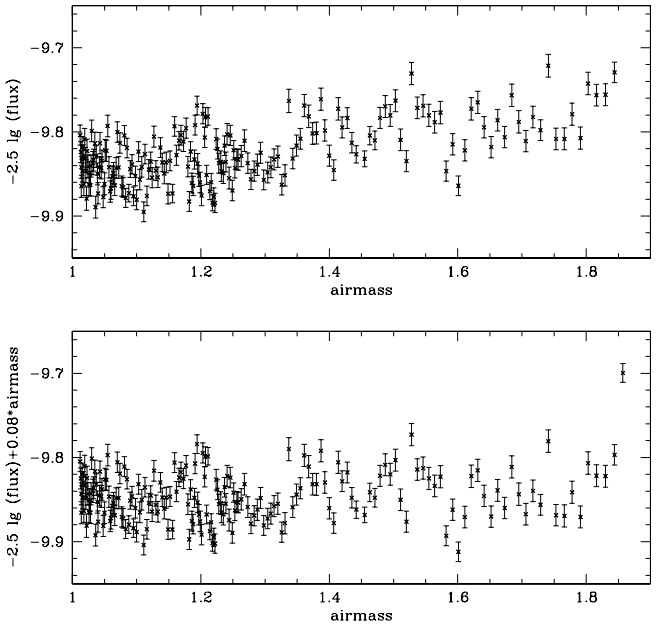

FIG. 4.—*Upper panel:* Air mass dependence measured by a possible elliptical galaxy of AC 118. *Lower panel:* Instrumental magnitude, air mass corrected, of the same galaxy. Notice the small scatter (0.03 mag) almost entirely due to photometric errors on the single measure.

during the night, and is equal to the value assumed by Persson et al. (1998) in defining standard magnitudes for the standard stars used here. Notice that the residual scatter in the data, after correction for air mass differential extinction, is 0.03 mag for the considered galaxy, of which 0.03 mag (i.e., almost all) are due to photometric errors in individual magnitude measures. The similarity of the expected and observed scatters gives a direct confirmation that the observing night was photometric and that the data reduction is accurate.

Aperture magnitudes have been used to measure the apparent flux of the standards, using the same aperture adopted by Persson et al. (1998) for the photometric standard stars, i.e., 10″ in diameter. The zero-point scatter derived from standard stars is 0.008 mag, of which 0.005 mag are due to photometric errors associated to the Persson et al. (1998) photometry.

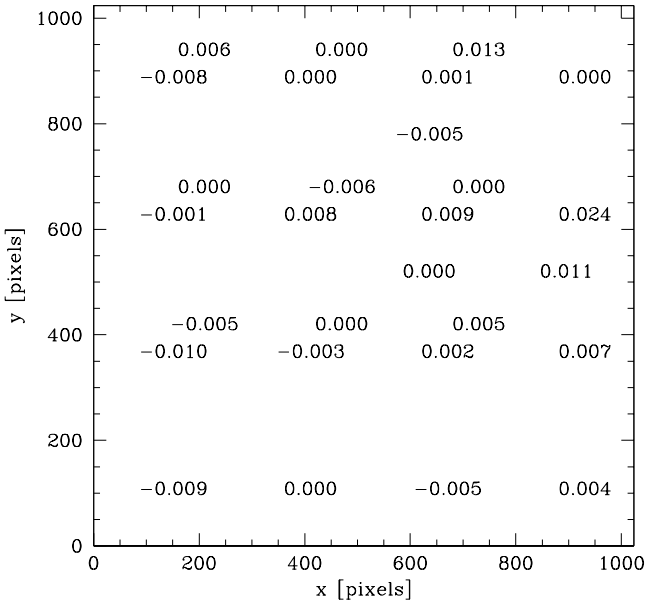

FIG. 3.—Illumination correction. Values indicate the deviation from a perfect flat-fielding (i.e., from 1 everywhere) and are located where measurements were performed. Typical measurement errors are 0.005

2.1.4. *Combining the Images and Final Details*

Images must be coaligned before co-adding. The jitter data reduction procedure uses cross-correlation techniques in the image domain to measure offsets with subpixel precision, adopting, as first estimates, the telescope spatial offsets written in the header of the FITS files. Images have been combined using the task `imcombine` under IRAF, since Eclipse does not fit our needs. Files containing the flux scaling (since AC 118 has been observed through different air masses), the bad pixel mask, and the relative spatial offsets were given in input. The task gives in output the composite image, the image of the measured dispersion among the input images and the number of pixels used (i.e., the exposure map in units of 1 minute). As "mean" for the `imcombine` task, we adopt a straight average allowing the rejection of up to one high and one low pixel value, to allow for the presence of cosmic rays or intermittent hot/cold pixels. We remember that `imcombine` deals only with integer shifts, and for this reason spatial offsets are rounded to the nearest integer. This fact inflates the final PSF by ~ 0.5 pixels.

Finally, a bright saturated star produces on the final image a row brighter than average (and a symmetric ghost row in the opposite image quadrants). A constant, computed as described in Andreon (1993) has been subtracted to these two rows.

The sky brightness ranged from 12.9 to 13.2 mag arcsec^{-2} during the night. The seeing, in the combined image, is 0.″75 (FWHM, $\simeq 2.5$ pixels). The sky noise in the fully exposed part of the image is 24.0 mag arcsec^{-2}.

2.2. *Control Field: Hubble Deep Field South*

Public images for the Hubble Deep Field South (HDF-S) have been taken in K_s with SOFI at NTT (Da Costa et al. 2000), i.e., with the same instrument, filter, and telescope as the AC 118 image. This ensures an almost perfect homogeneity of the data. A few characteristics of HDF-S images are listed in Table 1, together with those relative to AC 118 observations. Public images are already reduced. The reduction of these data follows the same lines described for AC 118 and makes use in large part of the same software used by us, i.e., Eclipse. The claimed photometric calibration has an error of 0.1 mag for HDF-S-1 and 0.05 mag for HDF-S-2 (Da Costa et al. 2000).

Differently from AC 118 images, HDF-S images have been spatially resampled and filtered during the combining phase, and for this reason the noise in the final image looks smaller than it really is. As a consequence, magnitude errors in Da Costa et al. (2000) are underestimated. In order to perform an uncorrelated measurement of the noise, as we did for AC 118 images, we binned the HDF-S images, thus reducing the correlation between adjacent pixels. Table 1 presents the fully corrected noise in AC 118, HDF-S-1 and HDF-S-2. Once corrected for correlated noise, the noises in the HDF-S and AC 118 images are consistent with the exposure times. Galaxy counts computed from these images agree with literature ones (Da Costa et al. 2000), as confirmed also by Figure 5.

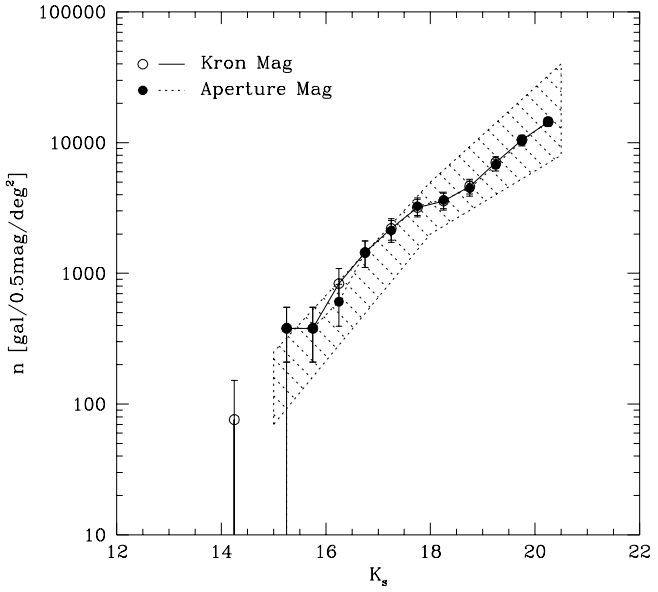

FIG. 5.—Galaxy counts adopting Kron (*open circles*) and aperture (*filled circles*) magnitudes in the HDF-S line of sight. Counts are identical almost at all magnitudes, and in particular at the bridge magnitude $K_s = 18$ mag. The hashed region delimits the locus occupied by literature galaxy counts in the K band, as estimated from the compilation presented in Fig. 1 of McCracken et al. (2000). The large amplitude of this region is due in part to heterogeneity of the data and reduction of the compared works.

2.3. *Detection and Completeness Magnitude*

Objects has been detected by using SEx version 2.1 (Bertin & Arnouts 1996). For AC 118 we made use of the rms map for a clean detection. Because of the varying exposure time across the field of each image, due to the dithering, we consider here only the central square areas listed in Table 1.

Galaxies have no well-defined edges; therefore their luminosity depends on how galaxy edges are defined. We adopt Kron magnitudes (see Kron 1980 for the exact definition, and Bertin & Arnouts 1996 for a software implementation), defined as the flux integrated in an area with size adapted to each galaxy. Unfortunately, Kron magnitudes depend sensibly on the determination of the object size, which is very difficult for faint objects and in crowded regions, such as the core of AC 118. Therefore, aperture magnitudes are adopted for faint objects. In detail, as a measure of the magnitude of the galaxies, magnitudes computed within 2.5 Kron radii are adopted for galaxies brighter than $K_s = 18$ mag and aperture magnitudes (at the 4.″4 aperture, which correspond to 24 Kpc) are used for fainter galaxies. Figure 5 shows that the two quantities give almost identical galaxy counts in a large magnitude range, and in particular near the bridge magnitude ($K_s = 18$ mag). Since the LF is computed by using galaxy counts, and not individual object magnitude, it is insensitive to differences between Kron and aperture magnitudes of each individual object.

In computing galaxy counts it is a standard practice to correct them for missing flux, i.e., for the flux not within the isophote or aperture. Usually, this correction is applied to all galaxies, independently of their luminosity. There is no reason for applying this correction for the LF determination, and furthermore, this correction has two shortcomings in our case. First of all, the absolute magnitude distribution of the galaxies of the same apparent magnitude differ in the two compared directions, because the sample in the cluster line of sight is the superposition of a volume complete (the cluster) and a flux limited sample (the fore/

TABLE 1

THE DATA

Parameter	AC 118	HDF-S-1	HDF-S- 2
Exposure time (minutes)	265	180	300
Seeing (FWHM, arcsec)	0.75	0.90	0.96
Fully corrected noise[b] (mag arcsec^{-2})	24.0	24.0	24.2
Complet. mag ($\phi = 4.''4$)	20.5	20.5	21.0
Galactic latitude (deg)	−81	−49	−49
Galactic abs. $E(B-V)$[a]	0.013	0.028	0.028

NOTE.—The full SOFI field of view is 5′ × 5′. The used field of view is 4.′52 × 4.′52.

[a] Color excess has been measured using *COBE*/DIRBE maps (Schlegel, Finkbeiner, & Davis 1998). Galactic absorption in K_s is $A_K = 0.2E(B-V)$ (Allen 1955).

[b] The sky noise is measured as the dispersion of adjacent pixels in the background, once the image is binned in pixels of 1″ for reducing the correlation between adjacent pixels in the HDF-S images.

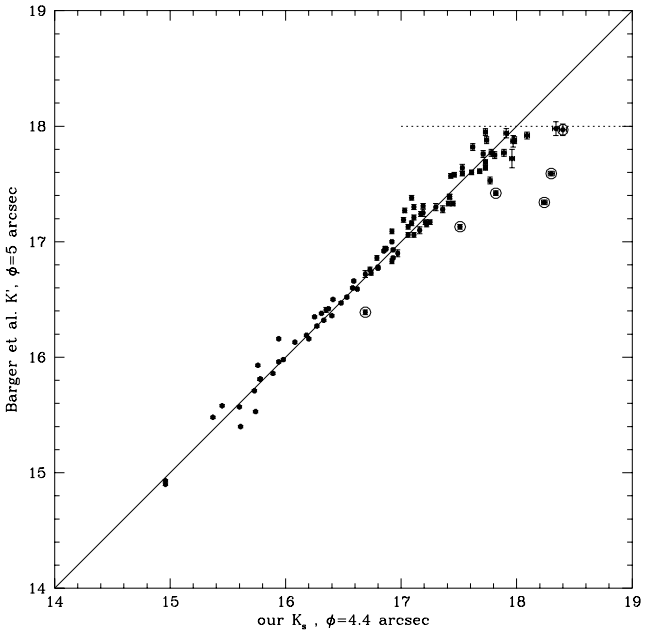

FIG. 6.—Comparison between Barger et al. (1996) K' magnitude in a 5″ aperture with our K_s magnitudes in a 4.″4 aperture for common objects. The line is the "one-to-one" relation, not a fit to the data. Outliers to the right of the line (*marked with a circle*) are pairs of objects, blended in Barger et al. (1996) image but resolved as separated components in our image. The horizontal dotted line marks the Barger et al. (1996) catalog limit.

background) while the control field is a flux limited sample. Thus, the luminosity correction is not the same, even at a fixed apparent magnitude, owing to both cosmological effects (cosmological dimming and K-correction at least) and the surface brightness profile of galaxies, which depends on the (unknown) absolute luminosity. Second, even under the optimistic hypothesis that corrections are perfectly known for each individual object, the catalog completeness is undermined by *bright* galaxies with low surface brightness (a long and thorough discussion on this topic is presented in Andreon & Cuillandres 2001).

The magnitude completeness is defined as the magnitude where objects start to be lost because their central brightness is lower than the detection threshold. It is measured as the brightest magnitude of the detected galaxies having central brightness equal to the detection threshold (see Garilli, Maccagni, & Andreon 1999 for details). For AC 118, the (5 σ) limiting magnitude is $K_s \sim 20.5$ mag in a 4.″4 aperture. Of course, many fainter and smaller objects are visible on the image, because the limiting magnitude is fainter using a smaller aperture, such as the "standard" 3″ aperture, or a 3 FWHM aperture.

2.4. *Star/Galaxy Classification*

Most previous similar studies have near-infrared images whose resolution is too coarse for allowing object classification as star or galaxy from the extent of the sources. Thus, observers were obliged to adopt the classification performed either on optical images of the cluster (e.g., Barger et al. 1996) or colors (e.g., de Propris et al. 1999). Given the good seeing and sampling of the AC 118 K_s image, the star/galaxy classification can be based on the object extent, as measured in the near-IR image itself, by adopting the SEx star/galaxy classifier. The very central area of AC 118 has been observed by the *Hubble Space Telescope* (Couch et al. 1998). Only a few stars (as classified by their compactness in the *HST* image) are brighter than the K_s completeness limits (AC 118 is at high Galactic latitude; see Table 1), and all of them are correctly classified as stars using the K_s image. Only a few galaxies, out of hundreds, are misclassified as stars because of their compactness. Therefore, *HST* confirms the goodness of our ground-based star/galaxy classification.

2.5. *Comparison to Literature Data*

AC 118 has been observed in the K' band by Barger et al. (1996). Figure 6 shows the comparison between their K' magnitudes, computed in a 5″ aperture, and our K_s mag, computed in a 4.″4 aperture for common objects. The line shows the one-to-one relation, and it is not a fit to the data. The agreement is good. Inspection of our image shows that outliers to the right of the one-to-one relation are pairs of objects, blended in Barger et al. (1996) and resolved here as separate objects, due to better seeing and sampling. A few of these objects are shown as inset in Figure 1.

3. THE AC 118 LUMINOSITY FUNCTION

The final image of AC 118 shows features which likely are gravitational arcs (Y. Mellier 1999, private communication), some of which are previously unknown. The brightest two are magnified in the lower panel of Figure 1. Other suspected lensed galaxies, not visible on the *HST* image because they fall outside its field of view, are likely present, but their confirmation requires a full lensing analysis of the image, which is outside our aims. The arcs visible in the near-infrared image and the other visible on the *HST* image point out two main mass concentrations: a central one, and another one offset to the northwest, thus confirming the binary structure suggested by the spatial distribution of the galaxies (Fig. 1). Inspection of public *ROSAT* HRI & PSPC images shows a similar binary structure, whose brighter clump is coincident with the assumed center of AC 118, while the second clump is at the northwest.

Figure 7 shows galaxy counts toward HDF-S and AC 118. Magnitudes have not been corrected for Galactic extinction, because the correction is very small ($< \sim 0.01$ mag and in any case negligible with respect to the HDF-S photometric zero-point error). Counts in the cluster direction are larger than in the field direction and the difference is large.

The cluster LF is the statistical difference between counts in the cluster direction and in the control field direction (Zwicky 1957; Oemler 1974). Its error should account for Poissonian fluctuations of counts along the cluster and field lines of sight and for non-Poissonian fluctuations of the counts, owing to the nonzero galaxy correlation function. We take into account the last term according to Huang et al. (1997). Thus, the statistical significance of any claim on the LF does not assume that fore/background in the cluster line of sight is the "average" one (or that observed in the control field), but instead takes into full account that the background counts fluctuate, from region to region, and fluctuate more than $\sqrt{n}$. We stress that background fluctuations enter twice in the error budget because the LF is given by a difference of two galaxies counts, each one subject to background fluctuations. For simplicity, we assume that errors of different nature can be added in quadrature (i.e., that standard error propagation laws can be used), and in

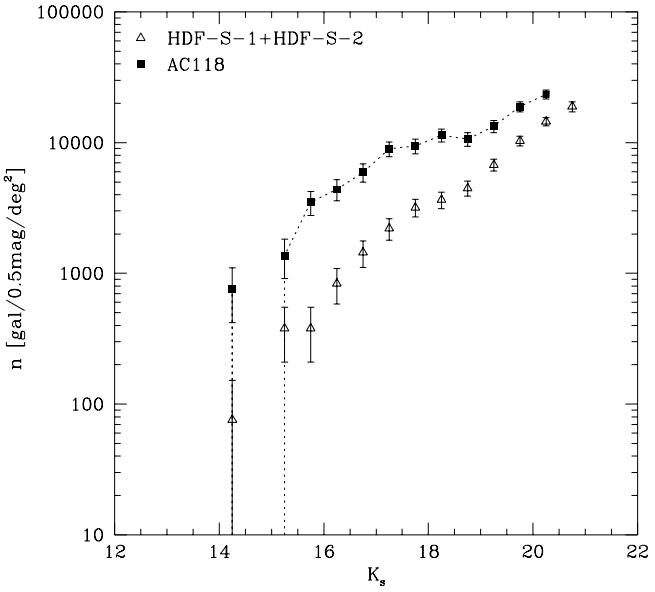

FIG. 7.—Raw galaxy counts in the HDF-S fields and toward AC 118. Error bars are simply taken as $\sqrt{n}$.

the error propagation we neglect the difference between Poissonian and Gaussian distributions.

In the very center of the cluster, galaxy density is high. Thus, in order to perform an accurate measure of the LF in this area, a crowding correction must be computed. For each magnitude bin, we consider as the area usable for the detection the one which is not filled by brighter galaxies. Since galaxies have no well-defined edges, we assign to each galaxy an excluded area equal to half their isophotal ($\mu \sim 24$ mag arcsec^{-2}) area. This correction turn out to be significant only in the central region of AC 118. Results are robust with respect to the implemented crowding correction.

Figure 8 shows the AC 118 global LF, i.e., those computed using all the $\sim 5' \times 5'$ field of view, corresponding to 2.66 Mpc^2 at the AC 118 redshift. The best-fitting Schechter (1976) function is also plotted. In order to take into account the amplitude of the bin, we fit the data with a Schechter function convolved with the bin width. The best-fit parameters are: $K_s^* = 15.3$ mag ($M_{K_s^*} = -26.0$ mag) and $\alpha = -1.2$, where α is the slope of the faint part of the LF, and M^* is the knee of the LF, i.e., the magnitude at which the LF starts to decrease exponentially. The confidence levels of the best-fit Schechter parameters are plotted in Figure 9. The AC 118 global LF is smooth, well described by a Schechter function ($\chi_\nu^2 = 0.7$) and has an intermediate slope, down to $K_s = 20.5$ mag ($M_{K_s} = -20.8$ mag), which is ~ 5 mag below M^*, well in the dwarf regime.[2]

Figure 10 summarizes two relevant features of the published cluster LFs in the near-infrared: it shows the magnitude limit reached as a function of the area surveyed. Points in the lower-right corner of the diagram are the most informative about the LF, because of the large area coverage and of the depth reaching the dwarf luminosity, but they are also the most expensive in terms of telescope time. The present study is marked by the point nearest to the lower-right corner of the graph. With respect to previous determinations, we explore at the same time one of the largest area and one of the deepest LFs, mainly because SOFI has 16 times more pixels, on average, than many previous instruments and because observations have been tailored for fundamental-plane studies, which require to measure the surface brightness profile of galaxies, not just their integrated magnitude. Thus, present data offer the possibility to study the environmental dependence of the LF and to sample possible effects on dwarf galaxies, in contrast to previous near-infrared cluster surveys that explored either smaller areas or a smaller magnitude range.

In order to search for a dependence of the LF on the environment, we compute the LF in two regions, centered on the two clumps of AC 118 (see Fig. 1). Each region has an area of ~ 0.5 Mpc^2, i.e., the typical area observed at comparable depth (see Fig. 10). The two LFs are plotted in Figure 11, together with their best Schechter fits. A Kolmogorov-Smirnov test shows that *data points* differ at 99.5% confidence level (i.e., they differ at $\sim 3\,\sigma$, but it should be remembered that this test makes no use of errors). The main clump of AC 118 is poorer in dwarfs and is richer in bright galaxies than the northwest clump. Figure 12 shows the confidence levels of the best-fitting Schechter parameters. *Assuming that the data are drawn from a Schechter function*, they differ at almost 95% confidence level (i.e., $\sim 2\,\sigma$, but now errors are taken into account). This plot confirms the previous finding: α is shallower in the main clump than in the northwest clump, indicative of an environment poor in dwarfs.

We now compare the LF computed in the main clump of AC 118 with that in the outer region. The outer region excludes both the two ~ 0.5 Mpc^2 regions centered on the two clumps and also a no-man's-land around the northwest clump (see Fig. 1). The galaxies in the main clump have an

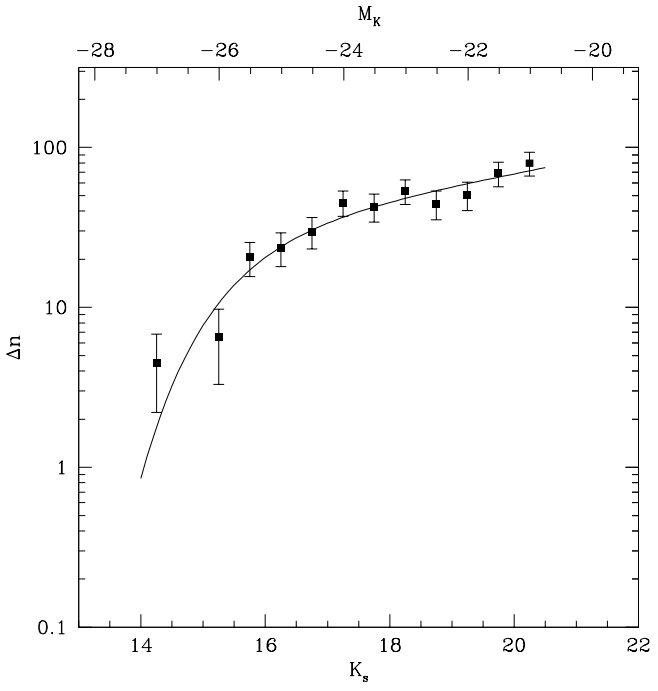

FIG. 8.—AC 118 global luminosity function. Error bars are $\pm 1\,\sigma$ and take into account both Poissonian and non-Poissonian fluctuations, i.e., include the cosmic variance of background galaxy counts. Both apparent and absolute magnitude scales are presented, as in most of the following figures.

[2] For the time being, we use the term "dwarf" for galaxies whose magnitude is $M > \sim M^* + 4$.

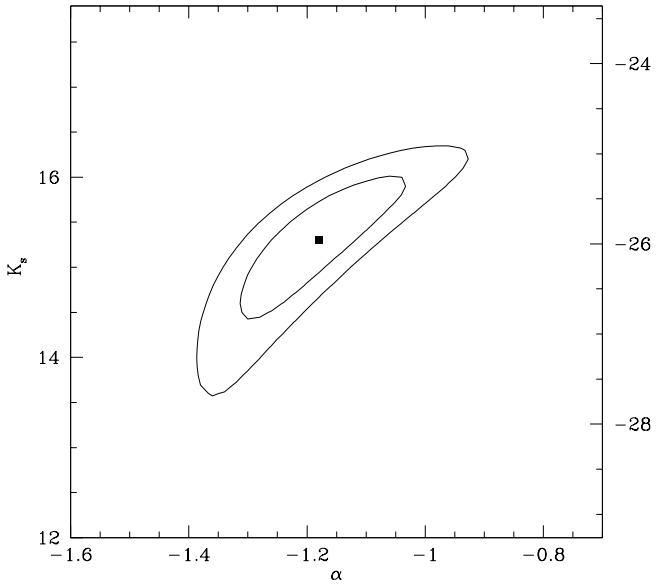

FIG. 9.—68% and 95% confidence levels of the best-fitting Schechter parameters for the global AC 118 LF. The filled square marks the best fit.

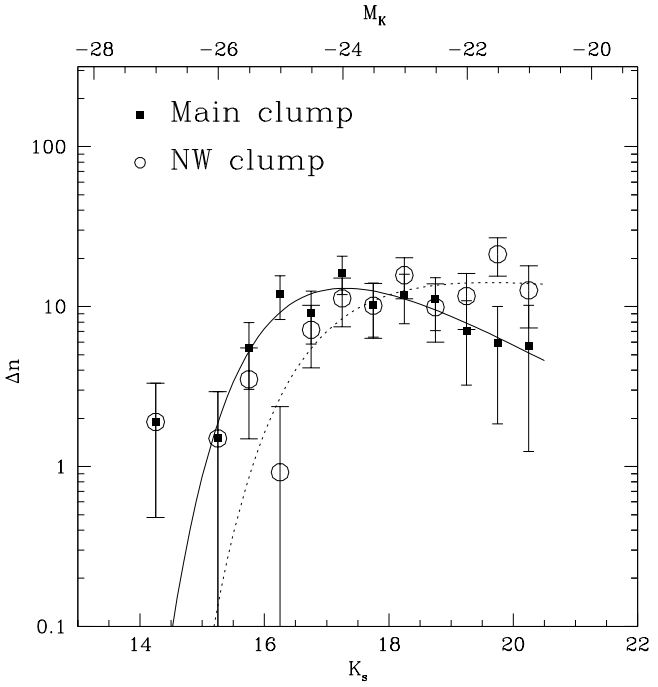

FIG. 11.—AC 118 LF of the two clumps. Filled squares (*open circles*) mark the LF computed for the main (northwest) clump. Error bars are as in Fig. 8. The two curves are the best Schechter fits (*solid line for the main clump, dotted line for the northwest clump*).

average projected distance of 180 kpc, while the galaxies in the outer region are 580 kpc away, on average, and 1.1 Mpc at most. Thus, the outer region is still well inside the cluster, as confirmed also by the fact that the galaxy overdensity is large enough for the LF to be computed with the differential counts method. Figure 13 shows that the inner and outer LFs differ (at more than 99.99999% confidence level according to a Kolmogorov-Smirnov test): there are far more dwarfs and somewhat fewer bright galaxies per typical galaxy (say $K_s \sim 18$ mag) in the outer region. In order to quantify these excesses, galaxies having $K < 17$,$17 < K < 19$, $K > 19$ mag are defined bright, typical and dwarf galaxies, respectively. These break magnitudes correspond, at the cluster redshift, to $M_K = -24.2$ and $M_K = -22.2$ mag, respectively. We found that the number of dwarfs per typical galaxy in the outer region exceeds the one observed in the central region by a factor $5.3^{+7.2}_{-2.3}$, where errors are quoted at 99.9% confidence level and are computed according to Gehrels (1996), i.e., by taking into account that the error on this ratio is partly binomial and partly Poissonian. The excess of bright gal-

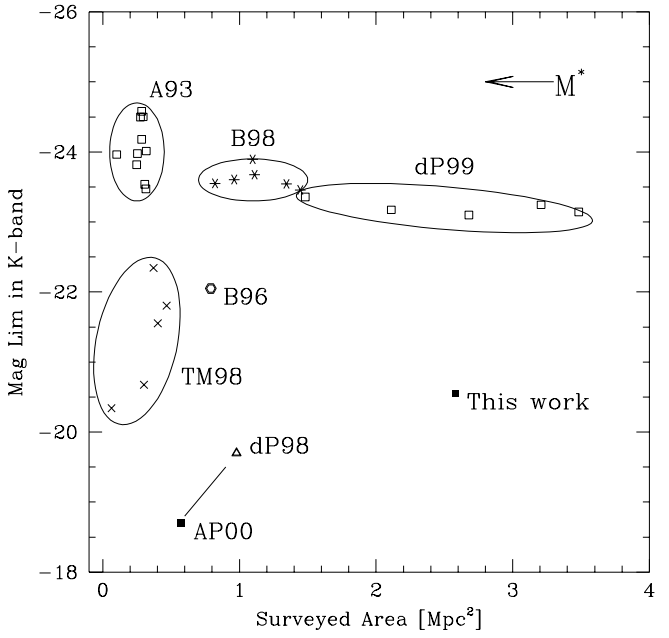

FIG. 10.—Rest-frame surveyed area vs. absolute magnitude limits for previous determination of the cluster near-infrared LF. LFs presented in Aragon-Salamanca et al. (1993), Barger et al. (1998, 1996), de Propris et al. (1998; 1999), Trentham & Mobasher (1998), and Andreon & Pelló (2000) are denoted as AE93, B98, B96, dP98, dP99, TM98 and AP00, respectively. The characteristic magnitude, M^*, of the Schechter LF is also marked. The line connect two different LF determinations of the Coma LF.

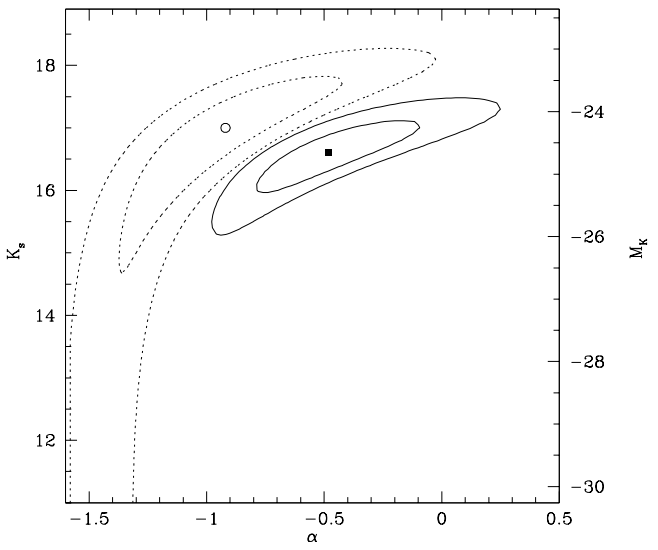

FIG. 12.—68% and 95% confidence levels of the best-fitting Schechter parameters for the main clump (*solid lines*) and northwest clump (*dotted lines*) of AC 118. The filled square and the open circle marks the best-fit values.

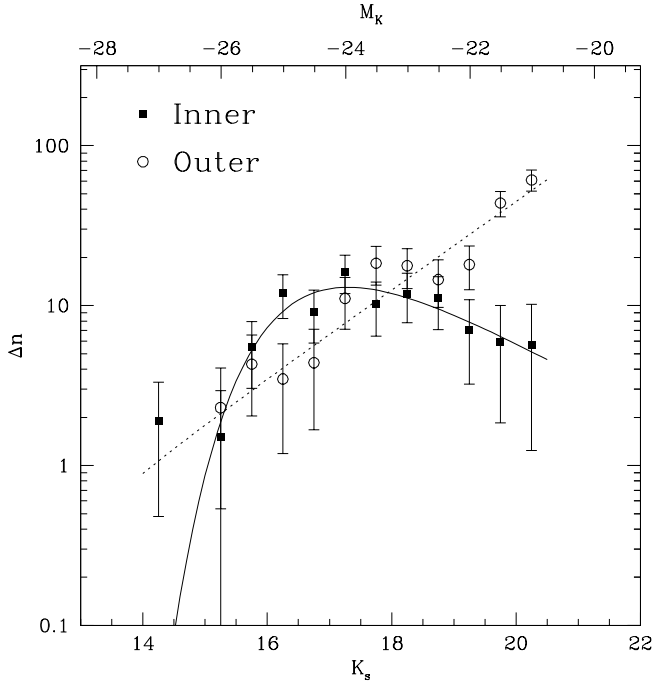

FIG. 13.—AC 118 LF of the inner and outer region. Solid squares (*open circles*) mark the LF computed for the inner (outer) region. Error bars are as in Fig. 8. The two curves are the best Schechter fits (*solid line for the inner region, dotted line for the outer region*).

axies in the main clump, with respect to the northwest region, is instead $2.6^{+5.1}_{-1.7}$ (99.9% confidence level).

Figure 14 gives the confidence levels of the best-fitting Schechter parameters for the inner and outer region. They are located in quite different parts of the diagram and point out the same differences shown in Figure 13. The same figure also shows that K^* is undetermined in the outer region. In other terms, the outer region LF can be accurately described by a power law.

There are some caveats in comparing values of one single best-fit parameter, say M^*, when they are computed by means of a fit with a function with three free parameters: a superficial inspection of the plotted confidence contours or of Table 2 would lead to a fairly different conclusion: M^* is brighter in the outer region and therefore bright galaxies are more abundant there, in apparent contradiction with our previous claims. However, errors on best-fit parameters are strongly coupled and one should be cautious when interpreting changes in one parameter, say M^*, when the two other parameters (α and ϕ^*) change at the same time. Since parameters are coupled, we emphasize the direct comparison of the data itself.

The excess of dwarfs in the outer region is large enough to make the number of dwarfs per typical galaxy in this region larger than the one observed for the global LF (which includes the outer region): we found $2.8^{+3.7}_{-1.5}$ more dwarfs here than over the whole area. With respect the SW region, the figure is $2.6^{+3.9}_{-1.5}$.

In conclusion, the near-infrared luminosity function of AC 118 depends on the considered cluster location: in the inner central region, dense in galaxies, there are more bright galaxies and fewer dwarfs per unit typical galaxy, than in the northwest clump or in the outer region. In other words, the AC 118 LF steepens going from high- to low-density regions. The outer region is the richest, among the three

TABLE 2

BEST-FIT VALUES

Region	K^*	α	ϕ	χ^2
Global.....	15.32	−1.18	31.21	7.21
Main clump	16.59	−0.47	30.74	4.33
Southwest clump.....	17.02	−0.91	19.24	10.05
Outer region	unconstrained	−1.69	0.21	10.01

NOTE.—All fits have 9 degrees of freedom and three free parameters, of which two (K^* and α) are interesting.

considered, in dwarfs and, at the same time, the poorest in very bright galaxies. The found differences among LFs measured in different cluster regions cannot be due to variations of background counts among the various cluster lines of sight because we have fully included in the error budget this source of error (which is the largest one).

3.1. *Comparison to Literature LF*

Barger et al. (1996) present the K' (virtually indistinguishable from K_s for our purposes, see Fig. 6) composite LF of the very central region of three intermediate redshift clusters at $z \sim 0.3$, one of which is AC 118. Their LF reaches $K' = 19$ mag, i.e., 1.5 mag brighter than our magnitude limit (compare B96 and our points in Fig. 10). They have in their composite sample $\sim$300 member galaxies to be compared to the $\sim$500 cluster galaxies of in our sample of AC 118 alone. Their best-fit parameters are $K' = 15.74 \pm 0.13$ mag and $\alpha = -1.0 \pm 0.12$. Since Barger et al. (1996) observed only the central region of the cluster, we consider here only the central area of AC 118 and we compare their best-fitting values to those we derived for the central clump (which of course includes just a fraction of our total sample of galaxies). We computed confidence levels for the best-fit of the composite LF of Barger et al. (1996) reading their data and errors from their Figure 7. Figure 15 presents our confidence levels for the main clump of AC 118 and for the composite sample of Barger et al. (1996). The two 1 σ confidence levels largely overlap, thus meaning that the two

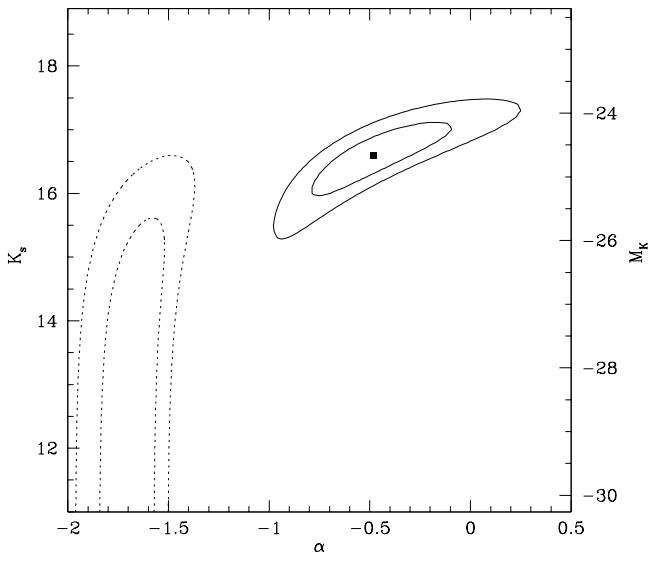

FIG. 14.—68% and 95% confidence levels of the best-fitting Schechter parameters for the inner region (*solid lines*) and outer region (*dotted lines*) of AC 118. The filled square marks the best fit of the inner region LF. The best fit for the outer region is undetermined.

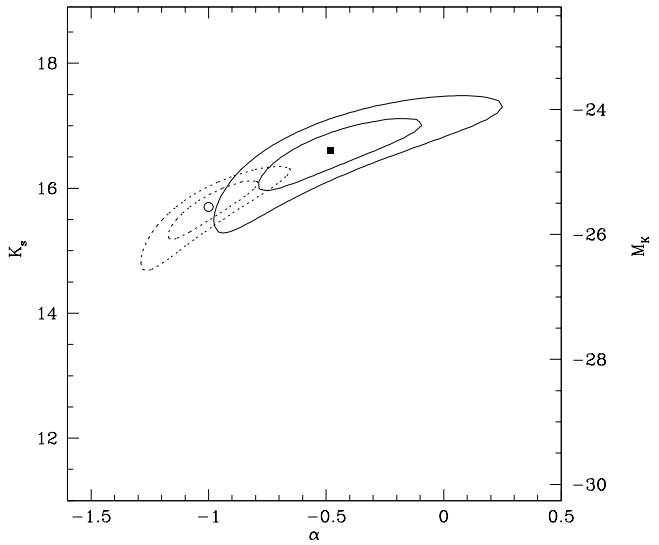

FIG. 15.—68% and 95% confidence levels of the best-fitting Schechter parameters for the inner region of AC 118 (*solid lines*) and the composite LF of three clusters at $z \sim 0.3$, including AC 118, presented in Barger et al. (1996) (*dotted lines*). The filled square and the open circle mark the best-fit values.

LFs are equal within the errors. This is expected, owing to the good agreement between individual magnitudes of galaxies in common shown in Figure 6.[3]

The K_s-band tightly maps the rest-frame H-band emission for objects at $z \sim 0.3$. Thus, without making any assumption on the K-correction value, we can compare the H-band zero-redshift LF of the Coma cluster (de Propris et al. 1998; Andreon & Pelló 2000) to our K_s band LF of AC 118.

The needed transformation is

$$M_{H_{z=0}} = -(m - M) + K_{z=0.3} + 0.09 \ .$$

The two Coma LFs are measured on different parts of the Coma cluster: de Propris et al. (1998) studied a ~ 1 Mpc^2 area around the cluster center and found a shallow slope ($\alpha = -1.0$), with an hint of steepening at faint magnitudes. Andreon & Pelló (2000) instead studied a ~ 0.6 Mpc^2 area off-centered by ~ 0.4 Mpc and found an overall slope of $\alpha = -1.3$. Both works found $M_H^* \sim -24.6$ mag. For AC 118, we found $K_s^* = 15.3$ to 16.8 mag depending on the considered area, which corresponds to $M_H^* = -26.2$ to -24.7 mag, in good agreement with Coma M_H^* when errors are taken into account. The trend for a LF shallower in the central region than in the other more external region suggested for Coma by Andreon & Pelló (2000) is confirmed for AC 118, with the major difference that data and analysis are homogeneous for the latter cluster, whereas for the former are not.

Figure 16 compares the LF computed in the outer region of AC 118 to the field LF, measured at $0.2 < z < 0.6$ (Cowie et al. 1996). These LFs are measured in two very different ways: the cluster LF is computed on a volume-limited sample, whereas the field LF is computed on a flux-limited sample (in fact, the Cowie et al. sample in not actually flux-limited, because it is incomplete and has a complex selection function). The two LFs, both concerning galaxies at intermediate redshift, have very similar shapes, and both conspicuously differ from the LF of the inner region of AC 118 shown in Figure 13. The similarity of these two LFs corroborates both the change of the LF parameters with the environment and the measured shape of field LF, which is based on a sample with a complex selection function. Environment seems to have played no role in modifying the near-infrared LF in the outer region of AC 118, because of the similarity of the LFs in the field and in the AC 118 outer region. Instead, Figure 13 shows that the environment modifies the LF shape at larger galaxies density or smaller clustercentric distances.

[3] Barger et al. (1996) quote errors of the best-fit parameters without specifying for how many free parameters there are. The comparison of our Fig. 15 to their errors shows that their quoted errors are for one free parameter. Adopting the usual convention of quoting error for the number of interesting parameter of the fit (see e.g., Avni 1976 or Press et al. 1993), which in the present case is two, i.e., α and M^*, the actual error on the slope of the LF is about twice larger than claimed by Barger et al. (1996).

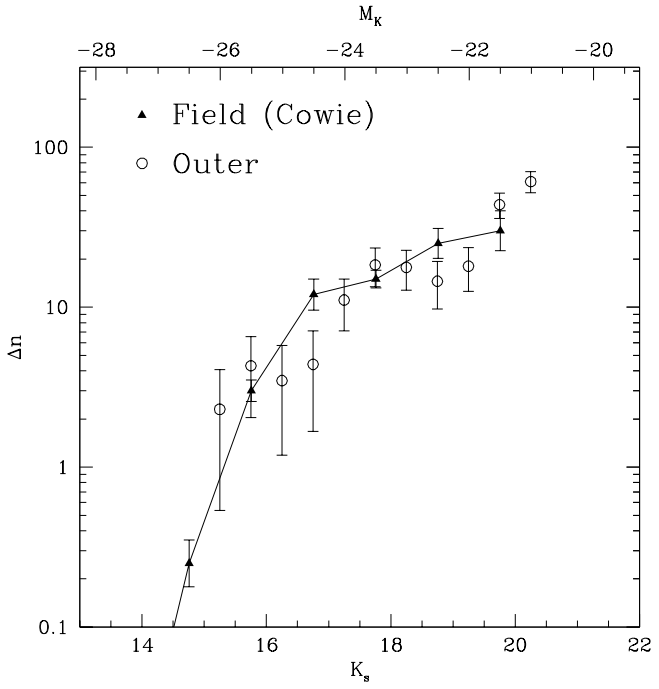

FIG. 16.—LF in the outer region of AC 118 (*open circles*) and in the field at $0.2 < z < 0.6$ (from Cowie et al. 1996; *filled triangles connected by a solid line*). The field LF has been vertically shifted to match the AC 118 LF.

4. DISCUSSION

The main result of this study is that the LF shape depends on location within the cluster. Among the studied regions, the cluster center, i.e., the main clump ($d \sim 180$ kpc), has many more bright galaxies per unit typical galaxy (say $K_s \sim 18$ mag, $M_H \sim -23.5$ mag), as shown in the previous section. The converse holds for dwarfs, which are less numerous in the center than elsewhere. The other observed clump, the second one in X-ray luminosity, presents LF characteristics intermediate between the central clump and the outer region. At an average clustercentric distance of ~ 580 kpc, the AC 118 LF is statistically indistinguishable, within the present errors, from the field LF at similar redshift.

Our definition of the main clump is sound: X-ray images and gravitational lensing distortion of background galaxies point out two main concentrations, of which the brightest in X-ray is also the one which we call main. Thus, our defini-

tion of main and center are independent and therefore unbiased by the presence of bright galaxies.

There is not anything like a near-infrared LF of AC 118, since it depends on the surveyed region. A similar result has been suggested for the Coma cluster by Andreon & Pelló (2000) from the comparison of heterogeneous near-infrared LFs computed by different authors on different portions of the Coma cluster. In the optical R band, Driver, Couch, & Phillips (1998) and Secker, Harris, & Plummer (1997) find a large variation in the ratio of dwarf to giant galaxies as a function of the clustercentric distances, with dwarfs more numerous at large ($r > 0.56$ Mpc) distances (or lower density regions). This trend is in agreement with the dependency of the slope of the LF with the density in the ~ 65 clusters studied by Garilli, Maccagni, & Andreon (1999). Because of the small *Hubble Space Telescope* field of view, it is not possible to measure whether the found variation of the LF is due to a change in the relative number density of galaxies of each morphological type (i.e., LFs of the morphological types are universal) or rather to luminosity changes of the individual galaxies (in that case the LFs of each morphological type depend on location), and should be deferred until *Hubble Space Telescope* images for a larger field will be hopefully taken. In the optical, the bright part of the luminosity functions of the morphological type are found not to depend on the considered environments, and differences in the optical LF are found mainly due to differences in the cluster morphological composition (Binggeli 1986; Jerjen & Tammann 1997; Andreon 1998).

The spatial dependence of the AC 118 near-infrared LF implies a luminosity segregation: bright galaxies are found preferentially in the cluster center. There are several claims (e.g., Driver et al. 1998; Secker et al. 1997) of a luminosity segregation for a few rich clusters, but this evidence is restricted to optical bands. In this paper, this evidence is extended to a near-infrared band. Since the near-infrared luminosity traces stellar mass (Bruzual & Charlot 1993), this result implies a mass segregation more tightly than under the usual assumption than optical luminosity traces mass: here we show directly that massive galaxies are found preferentially in the cluster center. Thus, more massive clumps are more tightly bound to the clusters, which is a general outcome of the simulations of a hierarchical universe (Kauffmann, Nusser, & Steinmetz 1997). The hostile cluster environment plays a role in shaping the AC 118 LF but only at small clustercentric radii (or high density), since the outer region AC 118 LF is quite similar to the field FL.

A possible not-ubiquitous cluster LF, i.e., varying with cluster radius, implies a dependency of the LF parameters (M^*, α) on the surveyed area and suggests caution in performing cosmological tests involving M^* as a standard candle, or in studying the galaxy evolution through a change in the best-fit LF parameters. Recently, de Propris et al. (1999) report a brightening of M^* with increasing redshift for their cluster sample, which is characterized by a surveyed area (in Mpc^2) varying with redshift in a complex way due to the variety of field of views of used instruments and sampled redshifts. They average a few cluster at each redshift, in order to reduce the impact of a not-ubiquitous cluster LF. Typically, areas range from 1.5 to 3.5 Mpc. However, the problem of a not-ubiquitous LF cannot probably be circumvented by choosing a fixed area in the cluster rest-frame because clusters have not standard size and shapes. Given the importance of determination of the evolution of M^*, we consider useful to check on a large sample of clusters the claim of a possible not-ubiquitous cluster near-infrared LF.

This work is part of a collaboration with M. Arnaboldi, G. Busarello, M. Capaccioli, G. Longo, P. Merluzzi, and G. Theureau. E. Bertin and N. Devillard are warmly thanked for their user friendly software (SEx and Eclipse) and their exhaustive answers to my detailed questions on technicalities about their software. Y. Mellier and E. Bertin helped me with setting SEx for the AC 118 image. I thank D. Maccagni for a careful reading of this manuscript and useful suggestions. A special thank goes to the anonymous referee for his very careful work and interesting feedback. The near-infrared observations presented in this paper have been taken during the NTT guaranteed time of Osservatorio di Capodimonte. This work is dedicated to the memory of my grandparents, Antonio and Maria Rapposelli.

REFERENCES

Abell, G. O. 1958, ApJ, 3, 211
Allen, C. W. 1955, Astrophysical Guantities (London: Athlone)
Andreon, S. 1993, in 5th ESO/ST-ECF Data Analysis Workshop, ed. P. J. Grosbol & R.C.E. Ruijsscher (Garching: ESO),. 219
———. 1998, A&A, 336, 98
Andreon, S., & Cuillandres, J.-C. 2001, ApJ, submitted
Andreon, S., & Pelló, R. 2000, A&A, 353, 479
Andreon, S., Pelló, R., Davoust, E., Domínguez, R., & Poulain P. 2000, A&AS, 141, 113
Aragon-Salamanca, A., Ellis, R. S., Couch, W. J., & Carter D. 1993, MNRAS, 262, 764
Avni, Y. 1976, ApJ, 210, 642
Balogh, M. L., Morris, S. L., Yee, H. K. C., Carlberg, R. G., & Ellingson, E. 1997, ApJ, 488, L75
Balogh, M. L., Schade, D., Morris, S. L., Yee, H. K. C., Carlberg, R. G., & Ellingson E. 1998, ApJ, 504, L75
Barger, A. J., Aragon-Salamanca, A., Ellis, R. S., Couch, W. J., Smail, I., & Sharples, R. M. 1996, MNRAS, 279, 1
Barger, A. J., et al. 1998, ApJ, 501, 522
Bertin, E., & Arnouts, S. 1996, A&AS, 117, 393
Binggeli, B. 1986, in Nearly Normal Galaxies, ed. S. Faber (Springer Verlag), 195
Bruzual, A. G., & Charlot, S. 1993, ApJ, 405, 538
Butcher, H., & Oemler, A., Jr. 1978, ApJ, 219, 18
———. 1984, ApJ, 285, 426
Colina, L., Holfeltz, S., & Ritchie, C. 1998, in ESO Conf. and Workshop Proc. 55, NICMOS and the VLT, ed. W. Freudling & R. Hook (Garching: ESO), 36
Couch, W. J., & Newell, E. B. 1984, ApJS, 56, 143
Couch, W. J., & Sharples, R. M. 1987, MNRAS, 229, 423
Couch, W. J., Barger, A. J., Smail I., Ellis R. S., & Sharples, R. M. 1998, ApJ, 497, 188
Cowie, L. L., Songaila, A., Hu, E. M., & Cohen J. G. 1996, AJ, 112, 839
Da Costa, L., et al. 2000, A&A, submitted (astro-ph/9812105)
de Propris, R., Eisenhardt, P. R., Stanford, S. A., & Dickinson M. 1998, ApJ, 503, L45
de Propris, R., Stanford, S. A., Eisenhardt, P. R., Dickinson M., & Elston R. 1999, AJ, 118, 719
Devillard N. 1997, Messenger, 87, 19
Driver, S. P., Couch, W. J., & Phillipps, S. 1998, MNRAS, 301, 369
Driver, S. P., & Phillipps S. 1996, ApJ, 469, 529
Ettori, S., & Rosat, A. C. F. 1999, MNRAS, 305, 834
Gaidos, E. J. 1997, AJ, 113, 117
Garilli, B., Maccagni, D., & Andreon S. 1999, A&A, 342, 408
Gehrels, N. 1986, ApJ, 303, 336
Huang, J.-S., Cowie, L. L., Gardner, J. P., Hu, E. M., Songaila, A., & Wainscoat, R. J. 1997, ApJ, 476, 12
Jerjen, H., & Tammann, G. 1997, A&A, 321, 713
Kauffmann, G., Nusser, A., & Steinmetz, M. 1997, MNRAS, 286, 795
Koo, D. C., & Kron, R. G. 1992, ARA&A, 30, 613
Kron, R. G. 1980, ApJS, 43, 305
Lumsden, S. L., Collins, C. A., Nichol, R. C., Eke, V. R., & Guzzo L. 1997, MNRAS, 290, 119
MacKay, C. D., et al. 1998, Proc. SPIE, 3354, 14
McCracken, H. J., Metcalfe, N., Shanks, T., Campos, A., Gardner, J. P., & Fong, R. 2000, MNRAS, 311, 707

Moorwood, A., Cuby, J.-G., & Lidman C. 1998, Messenger, 91, 9
Oemler, A., Jr. 1974, ApJ, 194, 1
Ostriker, G. 1993, ARA&A, 31, 589
Persson, S. E., Murphy, D. C., Krzeminski, W., Roth, M., & Rieke, M. J. 1998, AJ, 116, 2475
Phillipps, S., Driver, S. P., Couch, W. J., & Smith, R. M. 1998, ApJ, 498, L119
Press, W. H., Teukolsky, S. A., Vetterling W. T., & Flannery, B. P. 1993, Numerical Receipes (Cambridge: Cambridge Univ. Press)
Schechter, P. 1976, ApJ, 203, 297
Schlegel, D. J., Finkbeiner, D. P., & Davis, M. 1998, ApJ, 500, 525
Secker, J., Harris, W. E., & Plummer, J. D. 1997, PASP, 109, 1377
Simard, L., et al. 1999, ApJ, 519, 563
Smail, I., Ellis, R. S., Fitchett, M. J., Norgaard-Nielsen, H. U., Hansen, L., & Jorgensen, H. E. 1991, MNRAS, 252, 19
Smail, I., Ellis, R. S., Dressler, A., Couch W. J., Oemler, A., Jr., Sharples, R. M., & Butcher, H. 1997, ApJ, 479, 70
Trentham, N., & Mobasher B. 1998, MNRAS, 299, 488
Valotto, C. A., Nicotra, M. A., Muriel, H., & Lambas D. G. 1997, ApJ, 479, 90
Wilson, G., Smail, I., Ellis, R. S., & Couch, W. J. 1997, MNRAS, 284, 915
Zwicky, F. 1957, Morphological Astronomy (Berlin: Springer)